An estimate of global ocean circulation and heat fluxes

Alison M. Macdonald* & Carl Wunsch

Department of Earth, Atmospheric and Planetary Sciences, Massachusetts Institute of Technology, 77 Massachusetts Avenue, Cambridge, Massachusetts 02139, USA

ALTHOUGH **ocean circulation and the consequent exchange of heat and gases with the atmosphere exert a strong influence on climate, discussions of global circulation have previously been highly schematic[1–3] (invoking laminar flow patterns that ignore the turbulent nature of the real flow), non-quantitative and/or based upon mutually inconsistent regional studies[1–8]. Here we present a dynamically and kinematically consistent estimate of the magnitude and structure of global ocean circulation and its associated heat fluxes, derived by integrating hydrographic velocity data over the rapid spatial variations that they show. We find no single overturning cell, but instead a complex and probably time-varying circulation pattern. The simplest interpretation suggests that there are two nearly independent cells: one connecting overturning in the Atlantic Ocean to other basins through the Southern Ocean, and the other connecting the Indian and Pacific basins through the Indonesian archipelago.**

The data (temperature, salinity, oxygen and nutrient measurements along 23 hydrographic sections; Fig. 1) are combined using an inverse box model technique[9] to estimate the flow field. The model (Box 1) is represented by a set of noisy, under-determined linear simultaneous equations (993 equations in 1,930 unknowns) which are solved using a recursive, tapered weighted least-squares method[10]. The system is solved for estimates of the unknowns (geostrophic reference-level velocities and diapycnal fluxes) and their uncertainties. The solution cannot be regarded as definitive—it will change as new data are obtained. Many variations were tried; here we describe only our present best-estimate result. The best-estimate is a combination of statistical guidelines from the inversion with a certain amount of subjective oceanographic opinion.

The global circulation is a complicated turbulent flow whose details are not displayed here. But if the mass and corresponding property fluxes are integrated across ocean basins, a comparatively simple (but still complex) circulation emerges. Figure 2 is a simplified schematic representation of the general circulation for warm and cold temperature ranges and which should be temporally stable in its major elements.

Within the two temperature ranges shown, the integrated Atlantic-overturning cell carries an average of $(16 \pm 5) \times 10^9$ and $(17 \pm 5) \times 10^9\,\mathrm{kg\,s^{-1}}$, respectively. Fluid sinks at high latitudes in the North Atlantic, flowing out to the remainder of the ocean at depth. The estimated average magnitude of the Atlantic integrated cell is robust to most assumptions, but it is sensitive, for example, to the flux constraint placed upon the North Brazil current at 11° N, a variable and poorly known quantity[11].

Relatively warm waters flow northwards in the eastern South Atlantic and cross over to the western basin south of the Equator. The model produces a strong northward transport of upper-layer waters across the central and eastern portions of the northernmost section in the North Atlantic. Northward flows in the northeastern Atlantic have been suggested by some previous studies[12,13], but not by others[8]. This feature of the circulation could not be removed even by direct restrictions on the flow. Southward flow of deep waters, although generally seen in the western basins, is not always tightly tied to the western boundary.

Within the southwestern Atlantic, the deep waters from the north combine with the deep and bottom waters of the Weddell gyre region, and with the predominantly deep and intermediate waters entering from the Pacific through Drake Passage. Some of these waters turn northward and upwell within the eastern basin where there is a large heat gain by the ocean from the atmosphere (Fig. 1). Other waters flow into the Agulhas region of the Indian basin where they also upwell and return westward into the Atlantic in the form of eddies. The combined abyssal waters (mainly Circumpolar Deep Water with some Antarctic Bottom Water) move into the Indian and Pacific basins within the Antarctic Circumpolar current. In its passage through these basins, it appears that about $15 \times 10^9\,\mathrm{kg\,s^{-1}}$ of Lower Circumpolar Deep Water is replaced with intermediate water before returning to the Atlantic through Drake Passage. Most of this conversion takes place in the Indian basin.

Within the Indian basin, much of the deep water entering along the western boundaries of the sub-basins is returned in the Agulhas current. There is a conversion from colder (<3.5 °C) to warmer (>3.5 °C) waters to the north of 32° S. In the South Pacific, $(7 \pm 4) \times 10^9\,\mathrm{kg\,s^{-1}}$ enters at potential temperatures less than 0.8 °C, while across the Equator at 10° N, there is an increased northward flow of deep waters at temperatures greater than 0.8 °C. Much of the conversion from colder to warmer waters in the Pacific appears to occur well below the thermocline to the north of 10° N.

Much controversy exists[2,3,5,7,14,15] concerning the origin of waters which eventually form deep water in the northern North Atlantic:

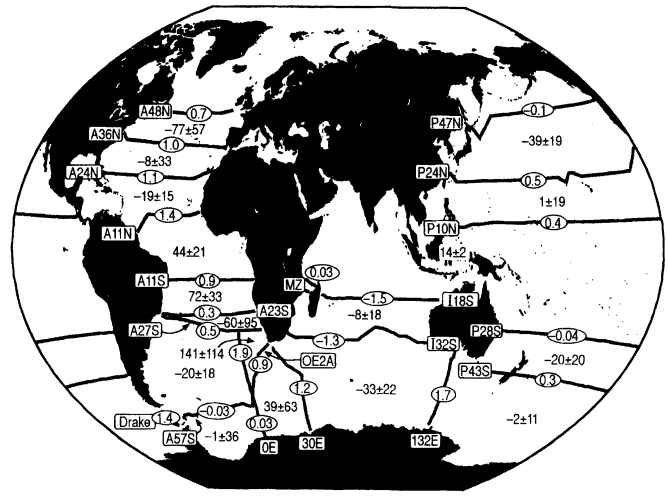

FIG. 1 Lines along which temperature, salinity, oxygen, and nutrient measurements were used. The data consist of 15 basin-wide zonal hydrographic sections plus four meridional sections in the Southern Ocean. With a short section across the Florida Straits and two sections in the Mozambique Channel, there are a total of 1,627 stations. Each section has been given a designation. Individual station positions are not shown but are densely spaced along the lines. All produced top-to-bottom values. Boxes in which mass and other properties (for example, salt, and silicate) are conserved, are defined by the lines, the continents, surfaces of constant potential density ('potential' densities are corrected for pressure effects) within the water column, the sea surface and the sea floor. To capture the character of the different water masses which exist around the globe, different potential density layer definitions are used in different regions. There are anywhere between 14 and 19 potential density interfaces in any particular box. Circled numbers are the integrated heat and temperature fluxes (in petawatts, PW, 10^{15} W) estimated from the flow field. Positive values indicate transport northwards or eastwards. The temperature fluxes across sections which support a net mass flux (that is, Drake, 0EN, 0E2A, 30E, 132E, P43S, P28S, I18S and I32S) are based on a 0 °C reference. The estimated uncertainty of these values is ~0.3 PW, except across 30E and 132E where the estimated uncertainty is 0.4 PW. The model estimated heat flux convergence (negative values) and divergence (positive values) in $\mathrm{W\,m^{-2}}$ are shown within the box interiors. A convergence represents a net heat loss to the atmosphere.

* Present address: College of Oceanic and Atmospheric Sciences, Oregon State University, Corvallis, Oregon 97331, USA.

BOX 1 Global ocean model

Components of model and constraints.

Mass and salt: conservation in all layers; Ekman convergence/divergence within each area = net top-to-bottom geostrophic outflow/inflow; geostrophic + Ekman flux across each section = net inflow/outflow.

Silica: conservation of silica below euphotic zone and above bottom.

Phosphate: conservation of phosphate and oxygen (1:138) below euphotic zone.

Net flux estimates: freshwater fluxes; from Baumgartner and Reichel[24] and Schmitt *et al.*[25] with an integration reference point at Bering Strait. Salt fluxes; based on Bering St., transport: $(0.8 \pm 0.6) \times 10^9\,kg\,s^{-1}$, $S = 32.5$. Antarctic Circumpolar current; $(142 \pm 5) \times 10^9\,kg\,s^{-1}$; North Brazil current; $(26.5 \pm 5) \times 10^9\,kg\,s^{-1}$; Florida Straits, $(30.8 \pm 0.5) \times 10^9\,kg\,s^{-1}$; Kuroshio, $(26.6 \pm 3.3) \times 10^9\,kg\,s^{-1}$; Indonesian Passage, $(10 \pm 10) \times 10^9\,kg\,s^{-1}$; Weddell Scotia area, net inflow of 0.1 ± 0.05 PW; Ekman fluxes, ECMWF winds (Note that the Ekman transport the 10° N section in the Pacific was taken from Wijffels[16].)

Topographic constraints: conservation of mass in the eastern basin of the North Atlantic, and in the deep equatorial Pacific; zero net flux below the sill depth (1) across the Walvis ridge and Agulhas plateau (2) within Mozambique basin and across the Southwest Indian ridge (3) in the Tasman Sea and the Philippine basin.

Weights: all equations are downweighted by their r.m.s. property value; the expected uncertainty of individual layers is $1 \times 10^9\,kg\,s^{-1}$; the expected uncertainty of top-to-bottom equations is $2 \times 10^9\,kg\,s^{-1}$; top-to-bottom equations are further downweighted by the uncertainty in the Ekman component; the surface layers are further downweighted by the magnitude of the Ekman component based on an estimated area of outcropping.

Model details.

The model is based on the assumptions of hydrostatic and geostrophic balance so that the so-called thermal wind equations apply. An added assumption is that property fluxes (for example, mass and salt) when integrated over trans-oceanic distances are time-independent over the data set duration (25 years), an assumption which is supported by the few available tests[26,27]. The models can be summarized as follows: (1) flows across the hydrographic sections are carried geostrophically and by the directly wind-driven surface Ekman layers. (2) The geostrophic flow is made up of two spatially varying parts—one of which is known, determined from the density field alone; the other is unknown, the so-called reference level velocity (integration constants) defined to be the geostrophic flow at an arbitrary, specified depth. (3) The Ekman mass fluxes are obtained from operational analysis wind stress values[28]. (4) Mass and other properties (for example, salt and silicate) are conserved within boxes defined by land, the sea surface and sea floor, the sections and surfaces of constant density up to observational and model error. Note that not all properties are conserved in all boxes. (5) The net fluxes across the sections are constrained with prior estimates and uncertainties. (6) The exchanges between boxes in contact in the vertical (that is, separated by constant density surfaces) are parametrized by a simple uniform flux over the box area. (7) The reference levels are a function of position and are chosen on the basis of prior estimates of depths of estimated weak flow. (8) All constraints are accompanied by an estimate of their uncertainty. The particular constraints used here are similar to those used by Macdonald[6], and the model is similar to others[7,9,29,30] used for regional studies. Details of the computations may be found in Macdonald[10].

whether having passed into and possibly through the Indian and Pacific basins, they mainly re-enter the South Atlantic through Drake Passage (the 'cold water' path) or, around the southern tip of South Africa (the 'warm water' path).

The complexity of the circulation indicated between the Atlantic and Indian sectors of the Southern Ocean suggests that simple, steady depictions will not produce viable quantitative estimates of the average westward flow entering the southeastern Atlantic. The model does show evidence, in the South Atlantic east of the Greenwich Meridian, of a strong northward transfer of surface and intermediate waters originating from Drake Passage. There is also ample evidence of water flowing westward to the south of the Cape of Good Hope and this water has similar properties to those found within the Benguela current. Taking the estimated strength of the flow between the Indian and Atlantic basins as typical would imply that the two routes are both important as sources for deep-water formation in the north. However, the uncertainties associated with the westward transport are large, as the 'warm water' flow is carried by a few strong eddy-scale features and this part of our results may well be temporally unstable, the two routes concerned possibly being dominant at different times.

Another controversy has concerned the strength of the Pacific–Indian flow through the Indonesian Passages (T_{PI} henceforth) and its relationship to the fluid returning to the North Atlantic. With no explicit constraints placed on the throughflow, the model produces an acceptable $T_{PI} = (11 \pm 14) \times 10^9\,kg\,s^{-1}$. However, the large uncertainty suggests that the model is capable of supporting both larger and smaller throughflows. Experiments using values of 0 and $20 \times 10^9\,kg\,s^{-1}$ (a range consistent with recent estimates[16–18]) as the T_{PI} constraint, have shown this to be true with neither extreme exhibiting any oceanographically unacceptable features.

A region of influence for T_{PI} was determined by finding those regions where significant mass flux changes occurred when T_{PI} was varied. Although effects were found within the Indian basin as far west as Madagascar, changes are not discernible in the Agulhas current and retroflection regions. The 'warm water' path for the Atlantic source appears therefore, to be independent of the magnitude of T_{PI}. Effects of changed throughflow do not affect the magnitude nor the properties of the mass flux through the Drake Passage either, so the 'cold water' path is also apparently uncoupled from T_{PI}. The model thus supports the hypothesis that the Pacific–Indian throughflow is not a significant part of a single overall global pathway.

The results are intrinsically complex, but can be interpreted as consistent with two global integrated cells. The first one connects Atlantic overturning to the Southern Ocean where the Antarctic circumpolar current carries lower deep waters to the Indian and Pacific basins where they are converted to upper deep, and intermediate, waters before returning to the Atlantic via Drake Passage. Some waters also re-enter the southeastern Atlantic having been warmed and upwelled in the Agulhas retroflection region. The second integrated cell connects the Pacific and Indian basins to the north and south of Australia. In this cell, deep waters pass into the Pacific, upwell in the north and return within the Indian basin as intermediate waters after passing through the Indonesian Passages. The two cells are found to be nearly independent, a result permitting a reinterpretation of the Gordon *et al.*[5] short-circuited warm water path.

Determination of the oceanic heat budget is important because it is a major component of the climate system. The mass conserving circulation estimate described here allows a calculation of the global oceanic heat budget (Figs 1 and 3). Heat fluxes across complete latitudinal circles are obtained at 47° N, 24° N and 30° S. At 30° S, the estimated heat flux of -0.9 ± 0.3 PW is dominated by a large (>1 PW) poleward temperature flux in the Indian basin and is not significantly affected by the magnitude of the T_{PI}. At 47° N, the net poleward heat flux of 0.6 ± 0.3 PW is dominated by the northward transport into polar regions within the Atlantic basin. The model estimate of 1.5 ± 0.3 PW calculated at 24° N is lower than, and only just consistent with, the 2 ± 0.3 PW of Bryden *et al.*[19]. Most of the discrepancy between our value and theirs

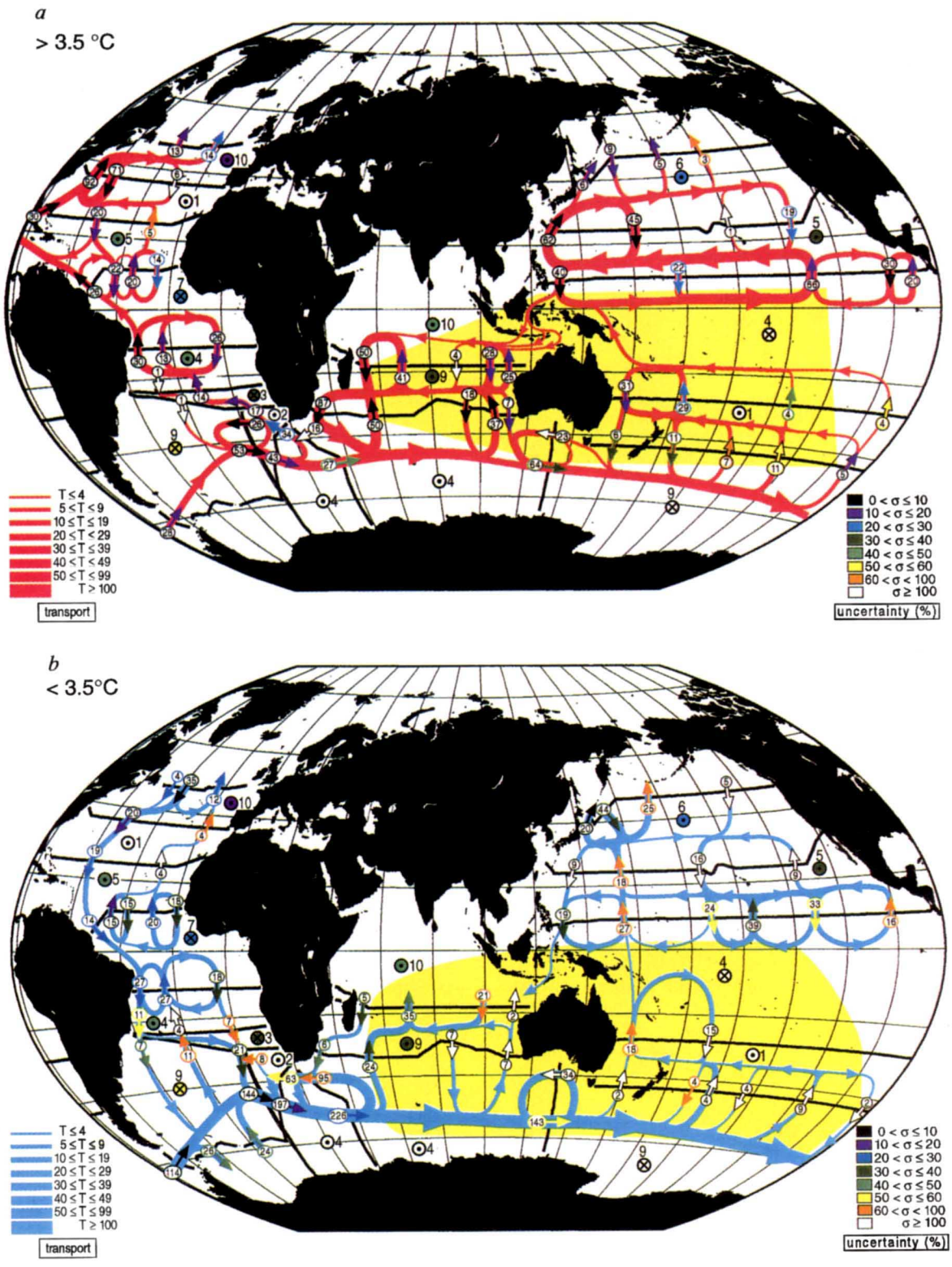

FIG. 2 Schematic representation of the global ocean circulation. Panel *a* illustrates the flow pattern (in red) of waters of potential temperatures greater than 3.5 °C; panel *b* illustrates the flow pattern (in blue) for potential temperatures less than 3.5 °C. (Potential temperatures are corrected for pressure effects.) The choice of the 3.5 °C isotherm is arbitrary. Its depth varies considerably around the globe, lying at about 2,200 m depth in the Atlantic, 1,200 m depth in the Pacific and 1,500 m depth in the Indian Ocean. It outcrops in the northern Atlantic at about 65° N and throughout the Southern Ocean between 50° and 60° S. The strengths of the transports T (in $10^9\,kg\,s^{-1}$) are indicated where they cross the sections and are further illustrated by line thickness (see key at left bottom). Colour shading of the vectors indicates, as a percentage, the ratio of the uncertainty in each transport estimate to the estimate itself (see key at right bottom). The vectors are placed geographically midway between the stations which have been integrated to obtain the transport values, and are not necessarily identifiable with strong local flows. Circles with dots indicate upwelling within a box through the 3.5 °C interface. Circles with crosses indicate downwelling. Shading within these symbols indicates the percentage uncertainty (as in the horizontal transport estimates) in the diapycnal transport estimates which are shown next to the symbols. Yellow shading indicates the deduced region of influence of the Pacific–Indian throughflow. Note that the uncertainty of the estimated pathways cannot be calculated from the model results and the temporal instability is likely to be great. The quasi-regularity of the scheme, particularly in the tropical Pacific, results from the very sparse data coverage combined with an attempt to minimize the inferred structure.

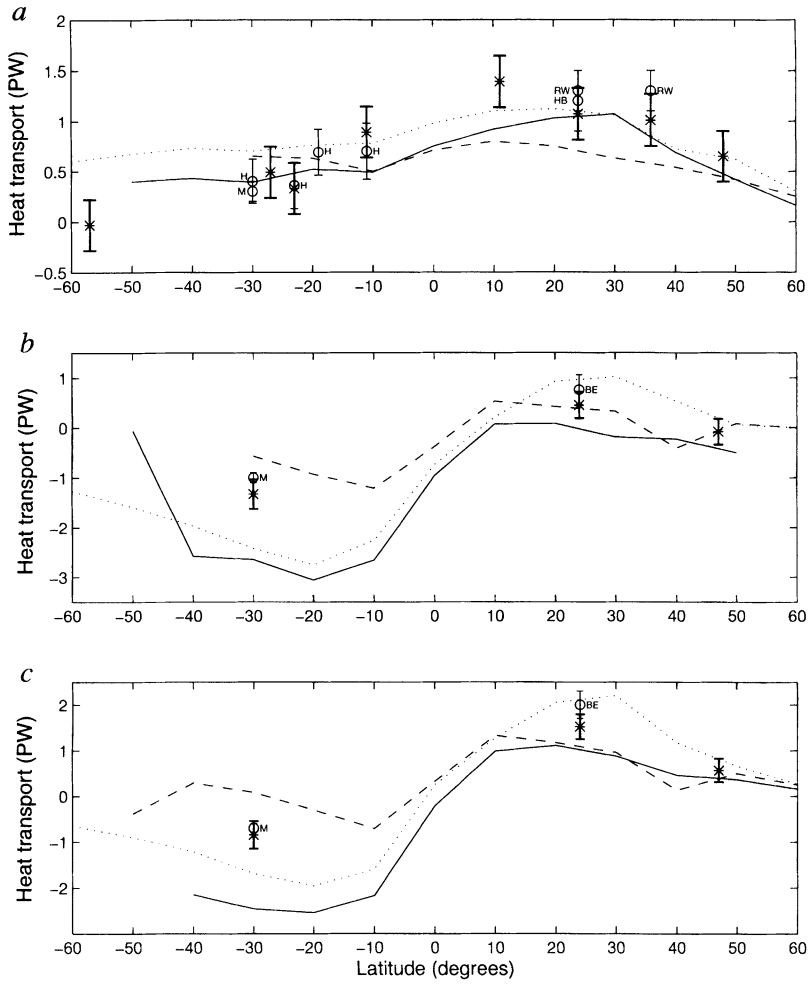

FIG. 3 Comparison of best-estimate model meridional heat flux estimates (asterisks with thick error bars) with previously published values (curves and open circles with thin error bars) which were based upon mass-conserving trans-oceanic observations and accompanied by uncertainty estimates. *a*, Atlantic Ocean; *b*, Indo–Pacific Ocean; *c*, All Oceans. Solid curve, Talley[31] from bulk formulae; dotted curve, Hastenrath[32] also from bulk formulae; dashed curve, the numerical model results of Semtner and Chervin[33] which have no error estimates. The reference initials represent the following: BE, Bryden *et al.*[19], HB, Hall and Bryden[34]; H, Holfort[35]; M, Macdonald[6]; RW, Rintoul and Wunsch[36]. All values are in PW. All the computed flux uncertainties are optimistic as they only represent the uncertainty in the absolute transport due to the uncertainty in the reference-level velocities. To roughly account for the difference between an instantaneous value and a long-term average an additional 0.25 PW (ref. 35) was included in the quoted values of uncertainty. Error bars on the previously published values do not include this contribution.

occurs in the Pacific and is due to differing estimates of the Ekman transport there.

The heat flux estimates presented here are robust, but sensitive to the initial estimates of the Ekman transport particularly at 10° N in the Pacific. The pattern of oceanic heat flux divergence (Fig. 1) shows net heat losses in the North Atlantic and Pacific oceans, heat gain around the equatorial regions and loss throughout much of the Southern Ocean. Southern Ocean divergence estimates are roughly consistent with previous ones[20,21]. There is strong oceanic heat gain in the small box to the southwest of South Africa—consistent with the findings of Bunker[22]. This pattern of heat flux divergences becomes a powerful test of atmospheric models[23] and must be regarded as a fundamental component of the present climate system. □

Received 15 January; accepted 5 June 1996.

1. Broecker, W. S. *Oceanography* **4,** 79–89 (1991).
2. Gordon, A. L. *J. geophys. Res.* **91,** 5037–5046 (1986).
3. Schmitz, W. J. Jr. *Rev. Geophys.* **33,** 151–173 (1995).
4. Boddem, J. & Schlitzer, R. *J. geophys. Res.* **100,** 15821–15834 (1995).
5. Gordon, A. L., Weiss, R. F., Smethie, W. M. & Warner, M. J. *J. geophys. Res.* **97,** 7223–7240 (1992).
6. Macdonald, A. M. *J. geophys. Res.* **98,** 6851–6868 (1993).
7. Rintoul, S. R. *J. geophys. Res.* **96,** 2675–2692 (1991).
8. Schmitz, W. J. Jr. & McCartney, M. S. *Rev. Geophys.* **31,** 29–49 (1993).
9. Wunsch, C. *Rev. Geophys. Space Phys.* **16,** 583–620 (1978).
10. Macdonald, A. M. thesis, Mass. Inst. of Technol./Woods Hole Oceanogr. Inst. Joint Program, Cambridge, MA (1995).
11. Friedrichs, M. A. M. & Hall, M. M. *J. mar. Res.* **51,** 697–736 (1993).
12. Martel, F. & Wunsch, C. *J. phys. Oceanogr.* **23,** 898–924 (1993).
13. Reid, J. L. *Prog. Oceanogr.* **33,** 1–92 (1994).
14. Döös, K. *J. geophys. Res.* **100,** 13499–13514 (1995).
15. Garzoli, S. L. & Gordon, A. L. *J. geophys. Res.* **101,** 897–906 (1996).
16. Wijffels, S. E. thesis, Mass. Inst. of Technol./Woods Hole Oceanogr. Inst. Joint Program, Woods Hole, MA (1993).
17. Fieux, M. *et al. Deep-Sea Res.* **41,** 1091–1130 (1994).
18. Meyers, G., Bailey, R. J. & Worby, A. P. *Deep-Sea Res.* **42,** 1583–1607 (1995).
19. Bryden, H. L., Roemmich, D. H. & Church, J. A. *Deep-Sea Res.* **38,** 297–324 (1991).
20. Georgi, D. T. & Toole, J. M. (suppl.) *J. mar. Res.* **40,** 183–197 (1982).
21. Guiffrida, M. R. thesis, Texas A&M Univ. (1985).
22. Bunker, A. F. *Mon. Weath. Rev.* **116,** 809–823 (1988).
23. Foreman, S. J., Alves, J. O. S. & Brooks, N. P. J., *Tech. Rep. 104* (Meteorological Off., Bracknell, UK, 1994).
24. Baumgartner, A. & Reichel, E. in *The World Water Balance* (Elsevier Science, New York, 1975).
25. Schmitt, R. W., Bogden, P. S. & Dorman, C. E. *J. phys. Oceanogr.* **19,** 1208–1221 (1989).
26. Fu, L. *J. phys. Oceanogr.* **11,** 1171–1193 (1981).
27. Roemmich, D. & Wunsch, C. *Deep-Sea Res.* **32,** 619–664 (1985).
28. Trenberth, K. E., Olson, J. G. & Large, W. G. *NCAR Tech. Note 338+STR* (National Center for Atmospheric Research, Boulder, Colorado, 1989).
29. Wunsch, C. *The Ocean Circulation Inverse Problem* (Cambridge Univ. Press, New York, 1996).
30. Wunsch, C., Hu, D. & Grant, B. *J. phys. Oceanogr.* **13,** 725–753 (1983).
31. Talley, L. *J. phys. Oceanogr.* **14,** 231–241 (1984).
32. Hastenrath, S. *J. phys. Oceanogr.* **12,** 922–927 (1982).
33. Semtner, A. J. & Chervin, R. M. *J. geophys. Res.* **97,** 5493–5550 (1992).
34. Hall, M. M. & Bryden, H. L. *Deep-Sea Res.* **29,** 339–359 (1982).
35. Holfort, J. thesis, Ber. Inst. Meeresk. Kiel (1994).
36. Rintoul, S. R. & Wunsch, C. (suppl. 1A) *Deep Sea Res.* **38,** 355–377 (1991).

ACKNOWLEDGEMENTS. We thank J. Toole, J. Marotzke, P. Malanotte-Rizzoli, H. Bryden and W. Schmitz for discussions; D. Spiegel, C. King and C. Gentemann for assistance with programming and data processing; and B. Brown for providing assistance in producing Fig. 2. This work is a contribution to the World Ocean Circulation Experiment and was funded in part by a NASA Global Change Fellowship, NASA and the USNSF.

CORRESPONDENCE should be addressed to A.M.M. (e-mail: alison@oce.orst.edu).